First-principles study of the dependence of ground-state structural properties on the dimensionality and size of ZnO nanostructures

Chun Li,[1,2] Wanlin Guo,[1,*] Yong Kong,[2] and Huajian Gao[3]

[1]*Institute of Nano Science, Nanjing University of Aeronautics and Astronautics, Nanjing 210016, China*
[2]*Max-Planck Institute for Metals Research, Heisenbergstrasse, 3, D-70569 Stuttgart, Germany*
[3]*Division of Engineering, Brown University, 182 Hope Street, Providence, Rhode Island 02912, USA*
(Received 20 November 2006; revised manuscript received 2 April 2007; published 18 July 2007)

The dimension- and size-dependent ground-state properties of ZnO systems are investigated through first-principles density-functional theory calculations. It is found that the effective elastic constants C_{33} of polar surface terminated ZnO nanofilms and [0001] oriented ZnO nanowires increase with structural size. For nanofilms, the effective C_{33} quickly approaches the bulk value and becomes almost stable when the film contains over six Zn-O double layers. For nanowires, the effective C_{33} is as small as around 16% of the corresponding bulk value when the diameter is very small, and it increases almost linearly to 88% of the bulk value when the diameter reaches about 2.4 nm. For ZnO nanoclusters with hexagonal prism structure, the original Zn-O double layers merge into single layers after relaxation. A shape-driven phase transition from the four-coordinate wurtzite to the six-coordinate rocksalt structure is found in a ZnO cluster with 48 atoms. Finally, a systematic energy analysis of all the above structures shows that the cohesive energies of the ZnO structures increase with both dimension and size.

PACS number(s): 73.22.−f, 73.90.+f, 73.61.Ga, 62.20.Dc

I. INTRODUCTION

Nanostructures of semiconducting materials are currently attracting a lot of interest as they are expected to play an important role in the development of future nanoscale technologies. As a typical II-VI semiconductor compound, zinc oxide (ZnO) has been receiving considerable attention due to its good optical, electrical, and piezoelectric properties. Recently, various functional ZnO nanostructures have been synthesized.[1–4] These nanostructures have attracted intense interest for their unique semiconducting, piezoelectric, and photoelectric properties. A number of studies have been devoted to understand their structures, properties, and novel behaviors experimentally and theoretically.[5–10]

To optimize the use of ZnO devices, it is essential to obtain a basic physical understanding of its properties. In spite of numerous experimental studies, corresponding theoretical work is necessary, especially for the low-dimensional nanostructures. For two-dimensional (2D) ZnO nanofilms, previous theoretical researches mainly focused on the structure and stability of the polar surfaces.[6,11,12] One-dimensional (1D) ZnO nanostructures have attracted considerable interest due to their great potential to serve as functional building blocks for various nanoscale devices.[13–16] Due to the interest in the variation of the electronic properties as a function of system size, there have been some theoretical studies devoted to the properties of zero-dimensional (0D) ZnO clusters.[17–20] However, systematical study on the dimension- and size-dependent properties of ZnO structures has not been reported until now.

In this paper, extensive density-functional theory (DFT) calculations are performed to systematically study the low-dimensional ZnO nanostructures with wurtzite structures from 2D to 0D. Corresponding properties of bulk ZnO are calculated for comparison. Significant size effects of the effective elastic constants C_{33} are found in ZnO nanofilms and

nanowires with limited sizes. Some other structures are formed in ZnO nanoclusters during full relaxation, especially the wurtzite-to-rocksalt phase transition observed in a cluster with relatively more dangling bonds. Finally, a detailed energy analysis is conducted to provide a better understanding for the dimension- and size-dependent ground-state properties of ZnO structures.

The remainder of this paper is organized as follows. In Sec. II, we describe the technical details for the calculations performed in this work. In Sec. III, we present and discuss our results for bulk and low-dimensional ZnO nanostructures from 2D to 0D, respectively. Whole energy analysis is also performed in the end of Sec. III. Finally, in Sec. IV, we present our summary and conclusions.

II. MODELING AND TECHNICAL DETAILS

ZnO is a tetrahedrally coordinated wide band gap semiconductor that crystallizes in the wurtzite structure. Bulk ZnO has been the focus of many theoretical analyses. Its crystal and electronic band structures have been studied by various total-energy methods, such as Hartree-Fock,[21] pseudopotential within local density approximation (LDA),[22] and self-interaction-corrected pseudopotentials.[23]

The calculations described in this work are performed using two DFT computational schemes: a plane-wave pseudopotential method implemented in the code ABINIT[24] and a pseudopotentials approach with localized atomic-orbital basis sets implemented in the code SIESTA.[25] (i) In ABINIT, we construct nonrelativistic optimized pseudopotentials using the code OPIUM for both Zn and O.[26] In details, the oxygen pseudopotentials are generated from a $2s^2 2p^4$ reference configuration with core radii r_c of 1.5 a.u. for both s and p orbitals; the zinc pseudopotentials are constructed with reference configuration $3d^{10} 4s^{1.75} 4p^{0.25}$. r_c values of 1.4, 1.4, and 2.0 a.u. are used for s, p, and d orbitals, respectively.[27]

In structural optimizations, convergence was assumed when the forces on ions are less than 5.0×10^{-6} hartree/bohr. (ii) In SIESTA, the corresponding pseudopotentials for both O and Zn are generated from the code ATOM[28] using the Troullier-Martins scheme,[29,30] where oxygen pseudopotential is generated using the same reference configuration as in the code OPIUM with the core radii of 1.15 a.u. for both s and p orbitals; the zinc pseudopotential is constructed with reference configuration $3d^{10}4s^2$. r_c values of 2.1, 2.1, and 1.9 a.u. are used for s, p, and d orbitals, respectively. The double-zeta polarized numerical atomic-orbital basis sets for both Zn and O are used. The convergence in force of 0.02 eV/Å (corresponding to 3.9×10^{-4} hartree/bohr) was guaranteed in the structural optimizations.

For bulk ZnO, the exchange-correlation (XC) effects are treated with both the LDA and the general gradient approximation (GGA), where we use the functional of Perdew *et al.*[31] In the bulk model, there are four atoms (two O atoms and two Zn atoms) in each unit cell. The k-point convergence was achieved with a $(6 \times 6 \times 4)$ Monkhorst-Pack[32] grid for both codes and XC functionals, and tests with up to $(12 \times 12 \times 8)$ k points have been made. In ABINIT, a plane-wave cutoff of 35 hartree was sufficient to get well-converged results by careful convergence tests. However, the corresponding value in SIESTA is much larger (250 hartree); the reason is that the computational technique implemented in SIESTA is not a real plane-wave method but an effective one. For both k-point sampling and the plane-wave cutoff used in our calculations, the relative energies are guaranteed to converge to 10^{-5} hartree.

For 2D ZnO nanofilms, we use the code ABINIT with LDA to calculate their elastic constants. The computational models of the nanofilms are generated by repeating certain number of the wurtzite cells along the [0001] direction. The vacuum region of about 10 Å between the slabs is chosen after careful convergence studies of the total energy, which is converged to 10^{-5} hartree. k-point convergence was achieved with a $(6 \times 6 \times 1)$ grid in the optimizations. To improve the accuracy, we chose k-point sampling of $(6 \times 6 \times 2)$ grid in the total-energy calculations. A plane-wave cutoff of 50 hartree was chosen in all the 2D cases. For each 2D structure, energy convergences down to 10^{-5} hartree were systematically guaranteed.

It is known that in the slab models, each Zn-O double layer exhibits a dipole moment perpendicular to the polar surfaces. However, there is a fundamental problem that these surfaces are unstable in the ionic model and should not exist. To stabilize the polar surfaces, a rearrangement of charges between the O- and Zn-terminated surfaces needs to take place, in which the Zn-terminated side becomes less positively charged and the O-terminated face becomes less negative. So in our calculations, the surface O atom at the $(000\bar{1})$ side and Zn atom at the (0001) side are replaced by artificial atoms with valency of 6.5 and 11.5, respectively. This so-called pseudoatom method has been used in the theoretical study of polar ZnO surfaces previously and reached reasonable results.[12]
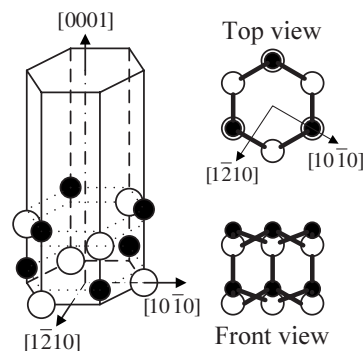
FIG. 1. Sketch of a ZnO nanowire or nanocluster model with 12 atoms. The top view and front view are presented on the right. Open and filled symbols represent oxygen and zinc ions, respectively.

In the cases of nanowires and nanoclusters, the code SIESTA with GGA is adopted in the calculations for its relatively low computational cost. To reduce the number of atoms in each unit cell and satisfy the hexagonal cross section, the three lattice vectors are designed orthogonal along the $[1\bar{2}10]$, $[10\bar{1}0]$, and [0001] directions, respectively, as shown in Fig. 1. Single k point was used in the structural optimization, and the convergence has also been tested using k-point samplings of $(1 \times 1 \times 2)$ and $(1 \times 1 \times 4)$ grids. The k-point sampling of $(2 \times 2 \times 6)$ grid was used in the total-energy computations. The energy convergence down to 10^{-5} hartree was guaranteed when the effective plane-wave cutoff of 250 hartree was chosen in the calculations.

III. RESULTS AND DISCUSSIONS

A. Bulk ZnO

Before we proceed to present the properties of low-dimensional ZnO structures, we first discuss bulk ZnO and compare the results of our calculations with published theoretical and experimental data. The original lattice constants used in our calculations are taken from the experimental unit-cell volume: a and c are 3.2595 and 5.2070 Å, respectively; the internal coordinate u, defined as the length of the bond parallel to the c axis in unit of c, is 0.3820. After full relaxation, the obtained lattice constants from the adopted codes and different XC functionals are listed in Table I. The present results agree well with the previous theoretical and experimental data, which are also listed for comparison.

The calculated cohesive energies of bulk ZnO from the energy calculations are also shown in Table I. Here, the cohesive energy, denoted as E_{coh}, is obtained by subtracting the total energy per ZnO unit (E_{ave}) at its equilibrium lattice constant from the energy of the corresponding isolated atoms. It is shown that the results obtained from ABINIT are much closer to the experimental value than that from SIESTA, which is mainly due to the different basis sets adopted in the two codes. In fact, there is nothing so special in SIESTA to keep from obtaining values of accuracy comparable to other packages with the pseudopotential approach since the localized atomic-orbital basis sets are adopted. However, in con-

TABLE I. Comparison between the present work and previous theoretical and experimental results for miscellaneous parameters of bulk ZnO.

	Codes	XC	a (Å)	c (Å)	c/a	u (Å)	V (Å^3)	C_{33}^{bulk} (GPa)	E_{coh} (eV)
Present results	ABINIT	LDA	3.2346	5.2121	1.6114	0.3808	47.23	212.5	−10.57
		GGA	3.3441	5.3069	1.5869	0.3829	51.40	171.4	−8.98
	SIESTA	LDA	3.1758	5.1775	1.6303	0.3748	45.06	357.8	−13.89
		GGA	3.2608	5.2698	1.6161	0.3773	48.40	282.1	−14.40
Previous results	Experimental		3.2498[a]	5.2066[a]	1.6021[a]		47.66[b]	210.9,[c] 211[d]	
			3.2496[e]	5.2042[e]	1.6018[e]	0.3819[e]	47.62[a]	208,[f] 196[g]	−7.52[h]
			3.2497[i]	5.206[i]	1.602[i]		47.59[e]	209.5[j]	
	Theoretical		3.286[k]	5.241[k]	1.595[k]	0.383[k]	49.14[l]	270,[n] 247[o]	−9.769[p]
					1.593[l]	0.3856[l]	46.692[m]	183,[s] 246[k]	−7.692[t]
					1.600[q]	0.383[q]	47.24[r]		
							47.678[s]		

[a]Measured by using energy-dispersive x-ray diffraction (EDXD) (Ref. 34).
[b]Reference 39.
[c]Ultrasonic measurement on single-crystal ZnO grown by chemical reaction in vapor state (Ref. 43).
[d]Surface Brillouin scattering on polycrystalline ZnO film deposited by rf sputtering on (100) Si substrate (Ref. 44).
[e]Measured by using x-ray diffraction (Ref. 35).
[f]Acoustic investigation technique on ZnO film deposited by rf magnetron sputtering on sapphire substrate (Ref. 45).
[g]Polarized Brillouin scattering on bulk ZnO single crystal (Ref. 46).
[h]Reference 48.
[i]Measured by using x-ray power diffraction (Ref. 36).
[j]Ultrasonic resonance method on ZnO single crystal (Ref. 47).
[k]Calculated by using *ab initio* periodic linear combination of atomic orbitals (LCAO) methods, based mainly on the Hartree-Fock Hamiltonian, with an all-electron Gaussian-type basis set (Ref. 37).
[l]Calculated by using first-principles periodic Hartree-Fock LCAO program (Ref. 21).
[m]Reference 40.
[n]Calculated using LDA (Ref. 41).
[o]Calculated using GGA (Ref. 41).
[p]Calculated using LDA (Ref. 40).
[q]Calculated by using *ab initio* quantum-mechanical level through the Berry phase scheme applied to delocalized crystalline orbitals and through the definition of well-localized Wannier functions (Ref. 38).
[r]Reference 41.
[s]Atomistic calculations based on an interatomic pair potential within the shell-model approach (Ref. 42).
[t]Calculated using GGA (Ref. 40).

sideration of computational cost, especially for the low-dimensional structures with supercell models, this code is more predominant than other approaches such as plane-wave pseudopotential or all-electron methods. In the last part of this section, detailed energy analysis of ZnO structures from 3D to 0D will be performed, where code SIESTA is used to obtain the whole set of data.

To compare the elastic property of low-dimensional ZnO structures with that of bulk ZnO, we first calculate the elastic constant C_{33} of bulk ZnO using the two codes with different XC functionals, respectively. The obtained values are also listed in Table I. In general, elastic modulus should be underestimated by GGA, which is also true in our calculations of each code. Although the results obtained from SIESTA are around 65% higher than that from ABINIT for both LDA and GGA cases, it is acceptable due to the high cohesive energy obtained from SIESTA as discussed above. Compared with the previous literature (some of those in Table I are derived from Ref. 33), the present results from ABINIT with LDA and SIESTA with GGA seem more accurate than the other two computational schemes. Therefore, they are used to calculate the effective elastic constants of ZnO nanofilms and nanowires in the following parts, respectively.

The calculated band structures for bulk ZnO at the optimized unit-cell volume is shown in Fig. 2. The results from ABINIT with LDA and SIESTA with GGA are shown, respectively. The Fermi energy is set to 0 eV. The band structures, especially the result in Fig. 2(a), are almost indistinguishable from that presented in Ref. 27, where details about the energy bands have been discussed. It should be noted that Fig. 2(b) shows a narrow gap between the bands from the Zn 3d orbitals (around −6 to −5 eV) and the O 2p orbitals (around −5 to 0 eV), which is not the same as in Fig. 2(a). This dif-
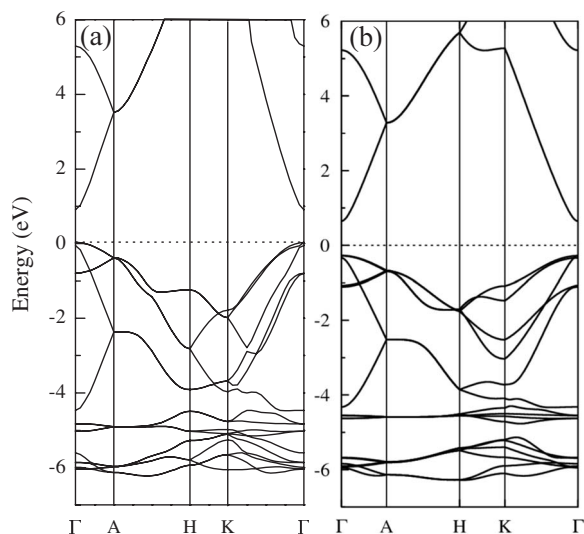
FIG. 2. Band structures of bulk ZnO calculated from (a) ABINIT with LDA and (b) SIESTA with GGA.

FIG. 3. (Color online) Normalized effective elastic constant C_{33}^{eff} of ZnO nanofilms (solid square) and nanowires (hollow circle) with respect to the corresponding bulk values.

ference comes from the local atomic-orbital method adopted in the latter case.

B. Two-dimensional ZnO nanofilms

ZnO crystallizes in the wurtzite structure, which does not have a center of inversion. Consequently, when the crystal is cleaved normal to the c axis in a manner which breaks the fewest interatomic bonds, two different polar surfaces are formed on opposite sides of the crystal, each having only one type of ion in its outermost plane. Thus, such a system may be considered to be a "slab" of material, with the Zn cation outermost for the (0001)-Zn surface and the O anion outermost on the (000$\bar{1}$)-O surface.[11] In our calculations, the slabs are created by stacking Zn and O layers along the c direction in the wurtzite structure, each layer containing one atom. Altogether there are six 2D structures involved in the present work. According to the number of Zn-O double layers, we denote them as 2S, 4S, 6S, 8S, 10S, and 12S, respectively. For example, 2S corresponds to two Zn-O double layers (i.e., four layers in total).

The normalized effective elastic constant C_{33} of ZnO nanofilms with respect to the bulk value is shown in Fig. 3. The results are obtained from the code ABINIT with LDA. The following computational steps are used. (i) First we perform full relaxations of the film models without any constraint. Large relaxations are found in both the Zn- and O-terminated surfaces, where the outmost double-layer distances are compressed by roughly 14%–30%. This agrees well with the results of previous researches.[6] (ii) Then the internal coordinates are further optimized with fixed film thicknesses after applying different strains. (iii) Next we calculate the total energies of the optimized structures with higher k-point sampling and larger energy cutoff, respectively. Finally, the effective C_{33} can be obtained by using the formula $C_{33}^{\text{eff}}=(d^2E/d\varepsilon^2)/V$, where E is the total energy, ε is the strain along the [0001] direction, and V is the effective volume of the unit cell. It is found that the effective C_{33}
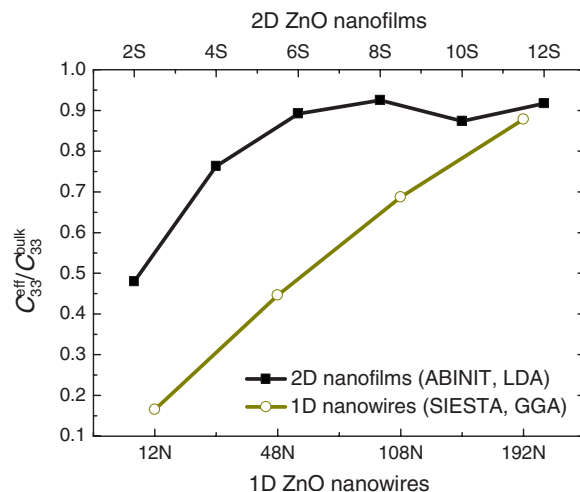
increases with slab thickness before reaching six Zn-O double layers, then the value remains almost unvaried and approaches the bulk value for the structures with six or more Zn-O double layers. This can be expected since the surface effect is quite strong when the nanofilm is very thin, while with increasing film thickness, the surface effect will trail off and the properties will approach those of the bulk case. Our surface energy analysis of the 2D structures has also confirmed that.[49]

C. One-dimensional ZnO nanowires

For the 1D ZnO nanostructures, [0001] oriented nanowires with diameters ranging from 0.4 to 3.0 nm are studied in our simulations. Here, the diameter is defined as the largest lateral distance between atoms. The thinnest nanowire studied in the present work contains 12 atoms in each unit cell, which we denote as 12N. Larger nanowires are generated by enlarging the hexagonal cross section along the lateral directions. We denote them as 48N, 108N, 192N, and 300N, respectively.

The effective elastic constants C_{33} of ZnO nanowires are calculated using the same formula used for ZnO nanofilms, while the total energies are obtained from the code SIESTA with GGA. The first full relaxation step is the same as that of the 2D case. However, since the 1D nanowires are infinite in the [0001] direction, no further relaxations are performed when we calculate the total energies with different strains. Figure 4 shows the normalized C_{33} of the 12N, 48N, 108N, and 192N nanowires with respect to the bulk value obtained from the same code and XC functionals. It is found that when the diameter of the nanowire is very small (0.4 nm), the effective C_{33} is only around 16% of the corresponding bulk value; with increasing nanowire size, the effective C_{33} increases almost linearly to 88% of the bulk value when the nanowire diameter is about 2.4 nm (192N). Compared with the 2D case in the same picture, the obtained elastic constants of ZnO nanowires also approach the corresponding bulk values with increasing size, but the size effect of the
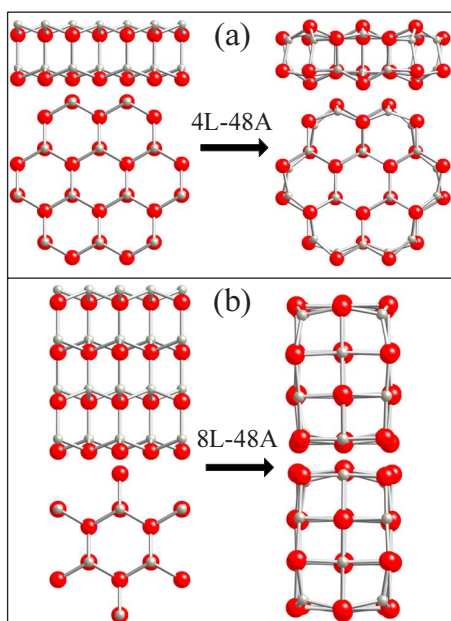
FIG. 4. (Color online) Side and top views of initial (left) and relaxed (right) ZnO nanoclusters: (a) 4L-48A and (b) 8L-48A. Large (dark) and small (gray) spheres represent O and Zn atoms, respectively.

FIG. 5. (Color online) Charge distributions in the cross sections of the optimized 8L-48A cluster, corresponding to the structure in the right panel of Fig. 4(b): (a) side-view and (b) top-view cross sections.

nanowires is more significant than that of the nanofilms. It is shown that dimension reduction in the [0001] direction or in the plane perpendicular to the [0001] direction of the wurtzite structure will weaken its elastic property, at least within the limited size studied in the present work. In fact, recent investigation[35] shows that Young's modulus in GaN nanowires with diameters smaller than about 90 nm decreases with diameter, and the value can be around 76% of bulk GaN when the diameter is about 36 nm. One possible reason is the increase of surface-to-volume ratio with decreasing diameter; the atomic coordination and cohesion near the surface are "poor" relative to bulk, and the increasing dominance of the surface would decrease the rigidity of the structure.[50] In addition, some atomic simulation results for Ni (Ref. 51) and SiSe$_2$ (Ref. 52) nanowires consistently demonstrate elastic modulus decreasing with decreasing diameter, where the diameters were of the same order as in the present calculations. Therefore, it is reasonable that the effective elastic constant of ZnO nanowires with such small diameters has a similar trend, just as the results from the present simulations.

D. Zero-dimensional ZnO nanoclusters

One of the major motivations in the study of ZnO nanoclusters is to develop a fundamental understanding of the material at the nanoscale as the properties and structures are often quite different from bulk and depend on size and shape as well.[20] In spite of numerous investigations on ZnO nanostructures, theoretical studies on the properties of ZnO clusters are rather scarce, especially for the clusters with hexagonal prism structures, which is a typical configuration observed in ZnO nanostructures. In the present calculations, the periodicity remaining in the [0001] direction of the 1D
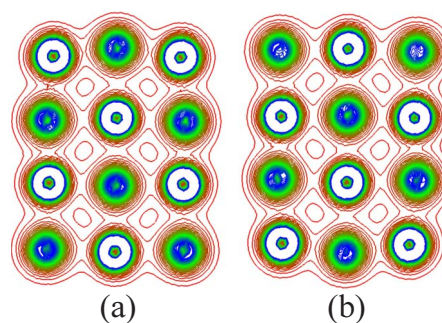
nanowires is removed, and then the ZnO nanoclusters with hexagonal prism structures are formed. Six nanoclusters with different sizes are studied in the present work. The smallest cluster studied in the present work contains 12 atoms of 4 layers, which we denote as 4L-12A. Larger clusters are generated by enlarging the hexagonal cross section or repeating the structures along the [0001] direction. We denote them as 4L-24A, 4L-48A, 8L-24A, 8L-48A, and 8L-96A, respectively.

Detailed structure optimizations and energy analysis of the above clusters can be found in our specific work.[53] Here, as representatives, the initial and relaxed structures of 4L-48A and 8L-48A clusters are shown in Fig. 4, from which we can draw the following common points for all the clusters studied in this work. (i) The original Zn-O double layers merge into single layers with both Zn and O atoms after optimizations. The reason is that cutting a cluster from the bulk ZnO destroys the periodicity along the [0001] direction in the wurtzite structure, which results in Zn- and O-terminated polar surfaces on each side of the cluster. During the relaxation, the original Zn-O double layers cannot maintain their configurations anymore; the Zn and O ions with opposite polarities in the same double layer move toward a common plane to find a relatively stable state. In fact, this phenomenon has also been found in recent first-principles calculations for single ZnO layers.[54] (ii) With increasing cluster size, size effect becomes evident on the boundaries, especially for the 4L-48A case as shown in Fig. 4(a). The atoms on the boundary have relatively more dangling bonds, so they try to find proper coordination during the relaxation.

It is interesting that the original hexagonal 8L-48A model shapes into a hexahedronlike cluster after relaxation, as shown in Fig. 4(b). Here, the final structure is shown with a clockwise rotation of 60° along the [0001] direction; we show it in the rotated direction for a clear exhibition. This reconstruction is a kind of wurtzite-to-rocksalt phase transition, which has been found in ZnO and other wurtzite semiconductors experimentally and theoretically when a certain pressure is applied.[40,55,56] To further investigate its electronic structure, we plot the charge distributions on two cross sections of the cluster, as shown in Fig. 5. The contours demonstrate that the charge distribution is quite different from

TABLE II. Energy analysis of ZnO systems (from 3D to 0D).

Systems		E_{ave} (eV)	E_{coh} (eV)
O atom		−2286.31	0.00
Zn atom			
Bulk		−2300.71	−14.40
2D (nanofilms)	2S	−2299.51	−13.20
	4S	−2299.95	−13.64
	6S	−2300.19	−13.88
	8S	−2300.32	−14.01
	10S	−2300.40	−14.09
	12S	−2300.45	−14.14
1D (nanowires)	12N	−2298.89	−12.58
	48N	−2299.83	−13.52
	108N	−2300.12	−13.81
	192N	−2300.27	−13.96
	300N	−2300.35	−14.04
0D (nanoclusters)	4L-12A	−2297.94	−11.63
	4L-24A	−2298.66	−12.35
	4L-48A	−2299.04	−12.73
	8L-24A	−2298.66	−12.35
	8L-48A	−2299.19	−12.88
	8L-96A	−2299.50	−13.19

FIG. 6. (Color online) Dimension- and size-dependent cohesive energies of ZnO structures.

shows that among the systems, bulk ZnO has the relatively lowest energy, indicating that it is more stable compared with the low-dimensional nanostructures.

Dimension- and size-dependent cohesive energies of all the ZnO systems are clearly exhibited in Fig. 6, where the results of the 0D ZnO clusters from Ref. 53 are redrawn for comparison of the dimensionality. It is also a complete presentation of the ground-state energy for all the ZnO structures studied in the present work. As a whole, the cohesive energy decreases with decreasing dimensions (from 3D to 0D). On the other hand, for the ZnO structures within certain dimension, the cohesive energies increase with increasing typical sizes. It is found that the dimension effect is more significant than the size effect within each dimension. It is interesting that there is an obvious step between the four-layer and eight-layer 0D structures, which demonstrates that clusters with the same size have similar cohesive energies. For the two pairs of clusters with the same numbers of atoms, the 4L-24A and 8L-24A clusters have almost the same configurations after relaxations, so they have exactly the same cohesive energy, while the 8L-48A cluster possesses a more favorable cohesive energy compared with that of the 4L-48A model due to the phase transition. This is reasonable because when the four-coordinate wurtzite structure shapes into the six-coordinate rocksalt one, much fewer dangling bonds result in lower surface energy. This also implies that by cutting out a stoichiometric cluster with more favorable structure, the dangling bonds should be as few as possible.

the original wurtzite structure, and a new six-coordinate rocksalt structure comes into being. In fact, the structural transformation in the ZnO nanoclusters is dominated by surface effects as proposed in the previous literature concerning CdSe nanocrystals.[56] Our simulations also show that in nanoclusters it is possible to stabilize structures that are unstable in the bulk by controlling the overall shape and their surface structure.

It should be noted that although some chemical bonds have been broken during the relaxations of 4L-24A and 8L-48A clusters, total-energy variations during the structure relaxations of the two clusters show that no remarkable energy barrier exists between the initial and final structures, because the initial cluster cutting directly from the bulk ZnO crystal is not stable with too many dangling bonds and too high initial energy state. During structure optimization, the initial energy is high enough to break the Zn–O bonds with monotonically decreasing energy to the final structure.

E. Energy analysis

In this section, we focus on the energy analysis of the whole ZnO systems involved in the present work. To remove the possible inconsistency between the two computational schemes, all the energies are obtained from the same code SIESTA with GGA, which has been discussed in Sec. III A for bulk ZnO. The average energy per ZnO unit (E_{ave}) and the cohesive energies (E_{coh}) of the ZnO structures with different dimensions and sizes are listed in Table II. The E_{ave} column

IV. SUMMARY AND CONCLUSIONS

Dimension- and size-dependent ground-state properties of ZnO structures from three-dimensional crystals to zero-dimensional clusters were systematically studied using first-principles density-functional pseudopotential approaches. Different computational schemes were involved in the present calculations to achieve a comprehensive understanding of the system. To make the discussions meaningful, we used as reference the results of bulk ZnO from each method and made a comparison of the lower-dimensional results and bulk results. In the case of bulk ZnO, we made detailed comparison with available experimental and calculated results to

provide a sound basis. The main results of the present investigation are an extensive set of reliable data for the ground-state properties of the various ZnO nanostructures (nanofilms, nanowires, and nanoclusters), which can provide a reference for future studies.

From the present calculations we draw the following conclusions. (i) The effective elastic constants C_{33} of the 2D and 1D ZnO structures are far lower than the corresponding bulk values when the nanofilm or nanowire is very thin, while both of them approach the bulk values with increasing size. (ii) Structural relaxations make the boundary effects remarkable in all the low-dimensional structures, such as the contractions of the outmost Zn-O double layers in nanofilms, small change of diameters in nanowires, and shape-driven phase transition in nanoclusters. (iii) The cohesive energy of the ZnO structures shows specific dimension and size depen-

dence. The dimension effect is more significant than the size effect within each dimension at nanoscale, and the values for the low-dimensional structures approach the bulk value with increasing size.

*Corresponding author. FAX: +86 25 84895827; wlguo@nuaa.edu.cn

[1] X. Y. Kong, Y. Ding, R. Yang, and Z. L. Wang, Science **303**, 1348 (2004).

[2] P. X. Gao, Y. Ding, W. Mai, W. L. Hughes, C. Lao, and Z. L. Wang, Science **309**, 1700 (2005).

[3] M. H. Zhao, Z. L. Wang, and S. X. Mao, Nano Lett. **4**, 587 (2004).

[4] I. Shalish, H. Temkin, and V. Narayanamurti, Phys. Rev. B **69**, 245401 (2004).

[5] M. Usuda, N. Hamada, T. Kotani, and M. vanSchilfgaarde, Phys. Rev. B **66**, 125101 (2002).

[6] B. Meyer and D. Marx, Phys. Rev. B **67**, 035403 (2003).

[7] L. G. Wang and A. Zunger, Phys. Rev. Lett. **90**, 256401 (2003).

[8] P. X. Gao and Z. L. Wang, Appl. Phys. Lett. **84**, 2883 (2004).

[9] Z. L. Wang, Mater. Today **7**, 26 (2004).

[10] Z. L. Wang and J. Song, Science **312**, 242 (2006).

[11] A. Wander, F. Schedin, P. Steadman, A. Norris, R. McGrath, T. S. Turner, G. Thornton, and N. M. Harrison, Phys. Rev. Lett. **86**, 3811 (2001).

[12] G. Kresse, O. Dulub, and U. Diebold, Phys. Rev. B **68**, 245409 (2003).

[13] X. F. Duan, Y. Huang, R. Agarwal, and C. M. Lieber, Nature (London) **421**, 241 (2003).

[14] Y. N. Xia, P. D. Yang, Y. G. Sun, Y. Y. Wu, B. Mayers, B. Gates, Y. D. Yin, F. Kim, and H. Q. Yan, Adv. Mater. (Weinheim, Ger.) **15**, 353 (2003).

[15] J. Song, X. Wang, E. Riedo, and Z. L. Wang, Nano Lett. **5**, 1954 (2005).

[16] Y. Ma, Z. Zhang, F. Zhou, L. Lu, A. Jin, and C. Gu, Nanotechnology **16**, 746 (2005).

[17] X. Lü, X. Xu, N. Wang, Q. Zhang, M. Ehara, and H. Nakatsuji, Chem. Phys. Lett. **291**, 445 (1998).

[18] Jon M. Matxain, Joseph E. Fowler, and Jesus M. Ugalde, Phys. Rev. A **62**, 053201 (2000).

[19] Jan-Ole Joswig, Sudip Roy, Pranab Sarkar, and Michael Springborg, Chem. Phys. Lett. **365**, 75 (2002).

[20] A. Jain, V. Kumar, and Y. Kawazoe, Comput. Mater. Sci. **36**, 258 (2006).

[21] J. E. Jaffe and A. C. Hess, Phys. Rev. B **48**, 7903 (1993).

[22] P. Schröer, P. Krüger, and J. Pollmann, Phys. Rev. B **47**, 6971 (1993).

[23] D. Vogel, P. Kruger, and J. Pollmann, Phys. Rev. B **52**, R14316 (1995).

[24] The ABINIT code is a common project of the Université Catholique de Louvain, Corning Incorporated, and other contributors (http://www.abinit.org).

[25] J. M. Soler, E. Artacho, J. D. Gale, A. García, J. Junquera, P. Ordejón, and D. Sánchez-Portal, J. Phys.: Condens. Matter **14**, 2745 (2002).

[26] http://opium.sourceforge.net/index.html

[27] N. A. Hill and U. Waghmare, Phys. Rev. B **62**, 8802 (2000).

[28] A. García, *ATOM User's Manual*, Version 3.2.2 (Universidad del País Vasco, Bilbao, 2006).

[29] N. Troullier and J. L. Martins, Phys. Rev. B **43**, 1993 (1991).

[30] N. Troullier and J. L. Martins, Phys. Rev. B **43**, 8861 (1991).

[31] J. P. Perdew, K. Burke, and M. Ernzerhof, Phys. Rev. Lett. **77**, 3865 (1996).

[32] H. J. Monkhorst and J. D. Pack, Phys. Rev. B **13**, 5188 (1976).

[33] Ü. Özgür, Ya. I. Alivov, C. Liu, A. Teke, M. A. Reshchikov, S. Dogan, V. Avrutin, S.-J. Cho, and H. Morkoç, J. Appl. Phys. **98**, 041301 (2005).

[34] S. Desgreniers, Phys. Rev. B **58**, 14102 (1998).

[35] H. Karzel, W. Potzel, M. Köfferlein, W. Schiessl, M. Steiner, U. Hiller, G. M. Kalvius, D. W. Mitchell, T. P. Das, P. Blaha, K. Schwarz, and M. P. Pasternak, Phys. Rev. B **53**, 11425 (1996).

[36] Robert R. Reeber, J. Appl. Phys. **41**, 5063 (1970).

[37] M. Catti, Y. Noel, and R. Dovesi, J. Phys. Chem. Solids **64**, 2183 (2003).

[38] Y. Noel, C. M. Zicovich-Wilson, B. Civalleri, Ph. D'Arco, and R. Dovesi, Phys. Rev. B **65**, 014111 (2001).

[39] C. H. Bates, W. B. White, and R. Roy, Science **137**, 993 (1962).

[40] J. E. Jaffe, J. A. Snyder, Z. Lin, and A. C. Hess, Phys. Rev. B **62**, 1660 (2000).

[41] R. Ahuja, Lars Fast, O. Eriksson, J. M. Wills, and B. Johansson, J. Appl. Phys. **83**, 8065 (1998).

[42] A. Zaoui and W. Sekkal, Phys. Rev. B **66**, 174106 (2002).

[43] T. B. Bateman, J. Appl. Phys. **33**, 3309 (1962).

[44] G. Carlotti, D. Fioretto, G. Socino, and E. Verona, J. Phys.: Condens. Matter **7**, 9147 (1995).

[45] G. Carlotti, G. Socino, A. Petri, and E. Verona, Appl. Phys. Lett. **51**, 1889 (1987).

[46] T. Azuhata, M. Takesada, T. Yagi, A. Shikanai, S. F. Chichibu, K. Torii, A. Nakamura, T. Sota, G. Cantwell, D. B. Eason, and C. W. Litton, J. Appl. Phys. **94**, 968 (2003).

[47] I. B. Kobiakov, Solid State Commun. **35**, 305 (1980).

[48] *CRC Handbook of Chemistry and Physics*, 58th ed. (CRC, Boca Raton, FL, 1977).

[49] C. Li, W. Guo, Y. Kong, and H. Gao, Appl. Phys. Lett. **90**, 033108 (2007).

[50] C. Y. Nam, P. Jaroenapibal, D. Tham, D. E. Luzzi, S. Evoy, and J. E. Fischer, Nano Lett. **6**, 153 (2006).

[51] P. S. Branicio and J.-P. Rino, Phys. Rev. B **62**, 16950 (2000).

[52] W. Li, R. K. Kalia, and P. Vashishta, Europhys. Lett. **35**, 103 (1996).

[53] C. Li, W. Guo, Y. Kong, and H. Gao, Appl. Phys. Lett. **90**, 223102 (2007).

[54] Z. C. Tu and X. Hu, Phys. Rev. B **74**, 035434 (2006).

[55] S. H. Tolbert and A. P. Alivisatos, Science **265**, 373 (1994).

[56] M. Grunwald, E. Rabani, and C. Dellago, Phys. Rev. Lett. **96**, 255701 (2006).